The growth and characterization of well aligned RuO_2 nanorods on sapphire substrates

2004 J. Phys.: Condens. Matter 16 8475

(http://iopscience.iop.org/0953-8984/16/47/002)

INSTITUTE OF PHYSICS PUBLISHING JOURNAL OF PHYSICS: CONDENSED MATTER

J. Phys.: Condens. Matter **16** (2004) 8475–8484 PII: S0953-8984(04)85869-7

The growth and characterization of well aligned RuO_2 nanorods on sapphire substrates

C C Chen[1], R S Chen[1], T Y Tsai[1], Y S Huang[1,4], D S Tsai[2] and K K Tiong[3]

[1] Department of Electronic Engineering, National Taiwan University of Science and Technology, Taipei 106, Taiwan
[2] Department of Chemical Engineering, National Taiwan University of Science and Technology, Taipei 106, Taiwan
[3] Department of Electrical Engineering, National Taiwan Ocean University, Keelung 202, Taiwan

Received 4 September 2004, in final form 27 October 2004
Published 12 November 2004
Online at stacks.iop.org/JPhysCM/16/8475
doi:10.1088/0953-8984/16/47/002

Abstract

Self-assembled and well aligned RuO_2 nanorods (NRs) have been grown on sapphire (SA) substrates via metal–organic chemical vapour deposition (MOCVD), using bis(ethylcyclopentadienyl)ruthenium as the source reagent. The surface morphology, structural, and spectroscopic properties of the as-deposited NRs were characterized using field-emission scanning electron microscopy (FESEM), transmission electron microscopy (TEM), selected-area electron diffractometry (SAD), x-ray diffraction (XRD), x-ray photoelectron spectroscopy (XPS), and micro-Raman spectroscopy. FESEM micrographs reveal that vertically aligned nanorods (NRs) were grown on SA(100), while the NRs on the SA(012) were grown with a tilt angle of $\sim 35^\circ$ from the normal to the substrates. TEM and SAD measurements showed that the RuO_2 NRs with square cross-section have the long axis directed along the [001] direction. The XRD results indicate that the RuO_2 NRs are (002) oriented on SA(100) and (101) oriented on SA(012) substrates. A strong substrate effect on the alignment of the RuO_2 NRs growth has been demonstrated and the probable mechanism for the formation of these NRs has been discussed. XP spectra show the coexistence of higher oxidation state of ruthenium in the as-grown RuO_2 NRs. Micro-Raman spectra show the red-shift and peak broadening of the RuO_2 signatures with respect to that of the bulk counterpart which may be indicative of a phonon confinement effect for these NRs.

1. Introduction

Fabrication of one-dimensional (1D) nanoscaled materials, such as nanowires, nanotubes (NTs), and nanorods (NRs), has attracted considerable attention owing to their fundamental

[4] Author to whom any correspondence should be addressed.

interest in science and potential in developing nanodevices [1, 2]. The development of nanodevices might benefit from the distinctive morphology, huge surface area, and high aspect ratio of nanotubes and nanorods. Down-scaling a broad range of materials, especially the oxide materials, to 1D nanoscopic structure is currently the focus of a rapidly growing scientific community. Wide band gap semiconductor ZnO nanorods are brilliantly prepared and well characterized [3–5]. The electrically insulating oxides of nanostructured SiO_2 [6], TiO_2 [7, 8], SnO_2 [9], GeO_2 [10], In_2O_3 [11], Ga_2O_3 [12], and VO_x [13] have also been synthesized and studied. Among the numerous metallic oxides, electrically conducting RuO_2 and IrO_2 belong to one family with unique properties, whose nanostructures are not well cultivated and merit extensive investigation [14, 15].

RuO_2 belongs to the family of transition metal dioxide compounds with a rutile structure. Because of its high electrical conductivity, chemical stability, and excellent diffusion barrier properties, it has found applications in thick film resistors [16, 17], electrode materials of electrochemical devices [18, 19]. It is also a candidate electrode material for ferroelectric random-access memory [20, 21], and a buffer layer for superconducting thin films [22]. In addition, RuO_2 NRs with the counterpart IrO_2 NRs [23] have been demonstrated to be candidate materials for field-emission cathodes of vacuum microelectronic devices and field-emission displays owing to the high chemical stability and high aspect ratio [24].

The synthesis of RuO_2 NRs has been previously reported, via a template-based method [25]. For practical applications, we develop a simpler method to fabricate large area and high density RuO_2 NRs on sapphire substrates. The 1D growth behaviour of RuO_2 is found to be highly correlated with the oxygen-rich ambient, growth temperature, and orientations of the substrate rather than the catalyst. The surface morphology, structural, and spectroscopic properties of the as-deposited NRs were examined by using field-emission scanning electron microscopy (FESEM), transmission electron microscopy (TEM), selected-area electron diffractometry (SAD), x-ray diffraction (XRD), x-ray photoelectron spectroscopy (XPS), and micro-Raman investigation. A strong substrate effect on the alignment of the RuO_2 NRs is observed, and the probable mechanism for the formation of NRs structure is discussed.

2. Experimental details

2.1. Growth of RuO_2 nanorods

A cold-wall and vertical-flow MOCVD system was used to prepare the samples on SA(100) and SA(012) substrates. The organometallic precursor bis(2,2,6,6-tetramethyl-3,5-heptanedionato) (1,5-cylooctadiene) ruthenium supplied by Strem Chemicals was utilized for chemical vapour deposition of RuO_2 samples. There were two different flow paths for oxygen carrier gas, connecting to the growth chamber. The first one is a bypass flow path, which is designed for controlling the chamber pressure, while the second is heated to the designated temperature and is used for transporting the source vapour to the growth chamber. Two independent temperature controllers were also mounted in the system to monitor the temperatures of the gas transfer line (T_t) and the precursor reservoir (T_p). Both T_t and T_p were kept at a constant value of 90–110 °C to avoid the condensation of the precursor during vapour-phase transport. High purity oxygen was used as both carrier gas and reactive gas with the flow rate adjusted to 100 sccm. During deposition, the substrate temperature and pressure of the CVD chamber were controlled at 450 °C and 10–50 Torr, respectively. The growth rate was controlled by adjusting the total pressure of the growth chamber and the partial pressure of the organometallic reagent.

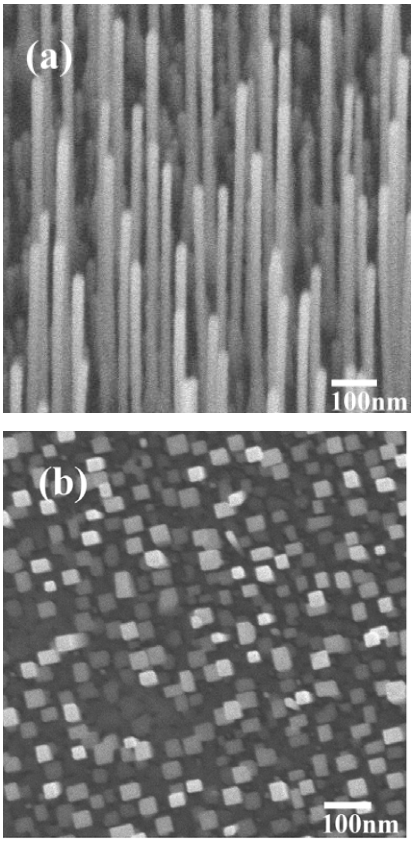

Figure 1. (a) The 30° perspective view and (b) top view FESEM micrographs of the vertically aligned RuO_2 square nanorods grown on SA(100) substrate.

2.2. Characterization of RuO_2 nanorods

The micrographs of RuO_2 samples were recorded using a JEOL-JSM6500F field-emission scanning electron microscope. TEM images and SAD patterns were recorded to check the nanostructure and preferential growth direction of the individual RuO_2 NRs (JEOL-200FXII TEM). X-ray diffraction patterns were recorded on a Rigaku RTP300RC spectrometer to examine the growth orientation over a large area. Surface compositions of RuO_2 NRs were analysed with x-ray photoelectron spectroscopy (XPS) using a Thermo VG Scientific Theta Probe system under the base pressure of 10^{-9} Torr. The Al Kα1486.68 eV line was the x-ray source and the Ag $3d_{5/2}$ line at 368.26 eV was the calibration reference. XPS peak positions and integrated intensities were obtained through curve fitting, using Thermo VG Scientific: Avantage v1.68 software [26]. Raman scattering spectroscopy was used to extract microstructural information about the RuO_2 NRs by using a Jobin-Yvon T64000 micro-Raman system, equipped with an Ar ion laser having an excitation wavelength of 514.5 nm which was focused on the sample using an optical microscope.

3. Results and discussion

As illustrated in figure 1, the FESEM images show vertically well aligned RuO_2 NRs grown on SA(100) substrate. The estimated edge size and the length of the NRs are around 20–40 nm

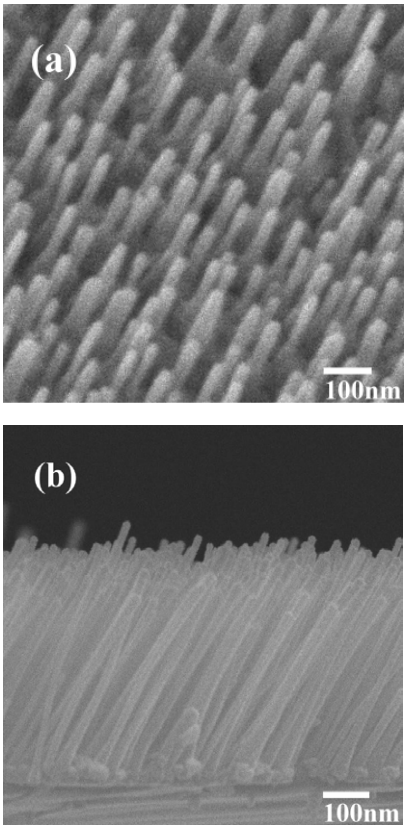

Figure 2. FESEM images of the well aligned RuO_2 nanorods grown on SA(012) substrate: (a) a 30° perspective view and (b) a cross-view. The self-assembled nanorods were grown with identical tilt angle (∼35°) from the normal to the substrate.

and 0.5–2.0 μm, respectively. The top view (figure 1(b)) images of the overall rods reveal clear solid squares with the edges parallel to each other. This result indicates that the rods standing on the substrate are perfectly vertical and follow the same in-plane orientation.

As illustrated in figure 2, the FESEM images show high density and well aligned RuO_2 NRs grown on SA(012) substrate. The self-assembled NRs were grown with identical tilt angle (∼35°) from the normal to the substrate. The estimated size, length, and packing density are 15–40 nm, 1–4 μm, and 175 ± 25 μm^{-2}, respectively.

Figure 3(a) shows the TEM image focused on a single RuO_2 nanorod. Figure 3(b) is the SAD pattern taken from the rod sidewall. The SAD pattern has been identified to be the [110] zone pattern, indicating that the rod walls belong to the {110} facets and the preferential growth direction of the RuO_2 rod is along the [001] direction (c-axis). A schematic plot of the RuO_2 rod is shown in figure 3(c).

Typical XRD patterns of the well aligned RuO_2 NRs grown on SA(100) and SA(012) substrates are shown in figures 4(a) and (b), respectively. As shown in figure 4(a), the single RuO_2(002) diffraction peak at ∼59.6° reveals the uniquely single directional growth of RuO_2 NRs along [001] for the sample grown on SA(100). As depicted in figure 4(b), a peak at around 35° is indexed to the (101) plane of rutile RuO_2, indicating that all the RuO_2(101) planes are parallel to the substrate plane. The results from electron diffraction and x-ray diffraction

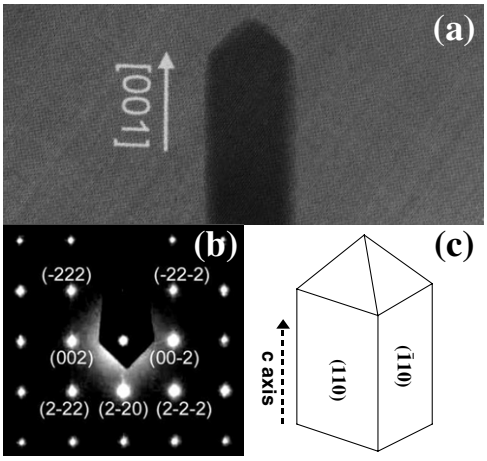

Figure 3. (a) The TEM image focused on a single RuO_2 nanorod. (b) The SAD pattern taken from the rod sidewall in (a). (c) A schematic diagram of the RuO_2 nanorod.

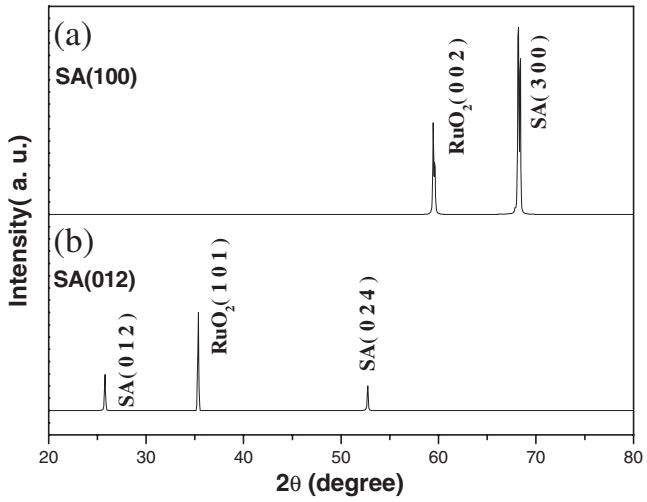

Figure 4. The XRD patterns for the RuO_2 nanorods grown on (a) SA(100) and (b) SA(012) substrates.

suggest that the growth mechanism of RuO_2 nanorods is the same as that for IrO_2 [14], even though the morphological appearances of these two conducting oxides are somewhat different.

Growth with (001) and (101) orientations of RuO_2 on SA substrates can be explained on the basis of the lattice relationship. The lattice parameters are $a = b = 0.449$ nm and $c = 0.311$ nm for RuO_2 [27], $a = b = 0.476$ nm and $c = 1.299$ nm for sapphire [28]. The lattice misfit at the interface produces strain energy when the RuO_2 is nucleated. The orientation that minimizes the lattice misfit and produces the smallest strain energy will be preferred. Schematic plots of the epitaxial relationships of RuO_2/SA(100) and RuO_2/SA(012) are shown in figures 5 and 6, respectively. The growth pattern results in the smallest lattice mismatch between the RuO_2 NRs and the substrates. According to the plot shown in figure 5, the in-plane orientation of RuO_2[100] along SA[010] shows a mismatch of $\sim -5.7\%$ while RuO_2[010] along SA[010]

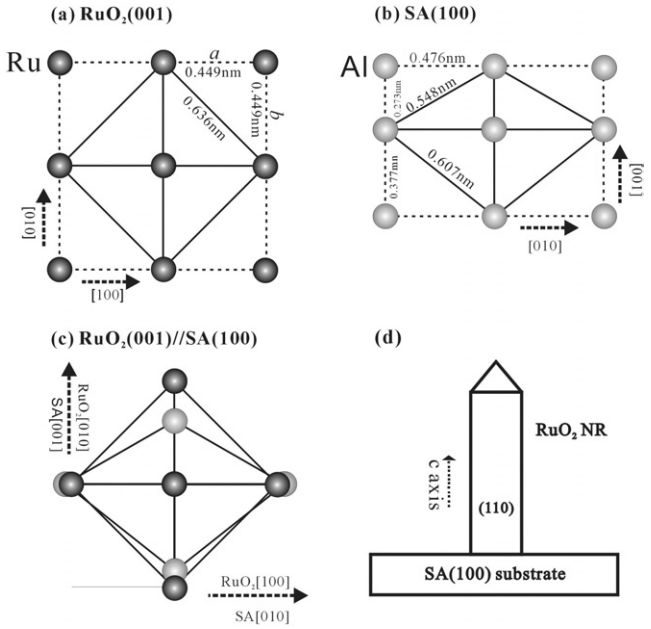

Figure 5. The schematic drawing of the epitaxial relationship between RuO_2 and SA(100): (a) the RuO_2(001) plane; (b) the SA(100) plane; (c) epitaxy of RuO_2(001)/SA(100). (d) The schematic diagram of the orientation relationship between the RuO_2 nanorod and the SA(100) substrate.

shows a mismatch of ∼38.1%. Therefore the overall orientation relationship between the RuO_2 nanorods and SA(100) can be described as $RuO_2(001) \parallel SA(100)$ and $RuO_2[100] \parallel SA[010]$. A schematic drawing of the epitaxial relationship of RuO_2 and SA(012) which resulted in a tilted growth of RuO_2 NRs is shown in figure 6. The lattice spacing of $RuO_2[0\bar{1}0]$ along SA[100] shows a mismatch of $\sim -5.7\%$ while $RuO_2[\bar{1}01]$ along $SA[\bar{1}\bar{2}1]$ shows a mismatch of ∼7.8%. Therefore the overall orientation relationship between the RuO_2 nanorods and SA(012) can be described as $RuO_2(101) \parallel SA(012)$ and $RuO_2[0\bar{1}0] \parallel SA[100]$.

Possible interpretation of the substrate effect on the tilted growth of RuO_2 NRs can be understood as follows: initially, the deposition of RuO_2 starts from the epitaxy of {101} planes on the SA(012) surface. Since the long axis of nanorods is along the [001] direction, the growth rate of (00l) planes should be the highest in this case. Then the tilted growth occurs along the [001] direction which is ∼35° from the normal to the SA(012) substrate or RuO_2(101) plane. This process leads to vertical 1D growth of RuO_2 NRs on the sapphire substrate and can likewise be explained by the initial RuO_2(001) nucleation on the SA(100) plane. Since the RuO_2(001) plane is normal to the SA(100) plane, under this anisotropic growth condition, the RuO_2(001) nuclei should elongate along {001} orientation and form vertically aligned NRs in the same direction. The schematic diagrams of the orientation relationship between RuO_2 NRs and SA(100)/SA(012) substrates are shown in figures 5(d) and 6(d), respectively.

The strong substrate effect on the alignment of the RuO_2 nanorods during growth has been demonstrated, where either the vertical or tilted alignment of the RuO_2 rods can be understood from the lattice misfits at the interface. However, the upward growth of rods from the interface with morphology of square cross-section is another issue of scientific interest. We shall discuss the possible origin of the morphology in terms of the *c*-axis directional growth mechanism. Directional growth of RuO_2 along the *c*-axis is always observed regardless of whether vertical

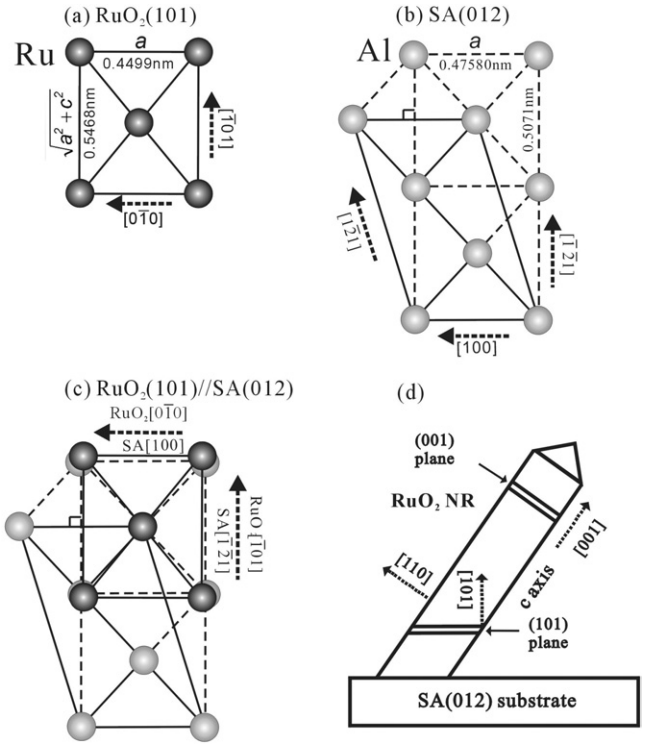

Figure 6. The schematic drawing of the epitaxial relationship between RuO_2 and SA(012): (a) the RuO_2(101) plane; (b) the SA(012) plane; (c) epitaxy of RuO_2(101)/SA(012). (d) The schematic diagram of the orientation relationship between the RuO_2 nanorod and the SA(012) substrate.

or tilted alignments of the square rods were formed. The [001] growth direction is preferred since the (002) plane is the least stable among (110), (101), and (002) planes [29]. In addition, the {110} planes are the most stable crystal planes for rutile structure materials [29]. Thus the RuO_2 growth proceeds to eliminate the (002) planes via forming its perpendicular {110} planes; accordingly the crystal elongates in the [001] direction with a square geometry.

The RuO_2 NRs were also examined using XPS to determine their composition, particularly the relative content of carbon impurities. Unfortunately the C 1s peak overlaps with Ru $3d_{3/2}$ at the binding energy ∼284 eV in the XPS survey scan, thus making direct measurement of the carbon content impossible. However, the Ru $3d_{5/2}$ peak at ∼280 eV does not overlap with any carbon signals, and the $3d_{5/2}/3d_{3/2}$ peak intensity ratio of RuO_2 NRs was approximately 3:2, which closely corresponds to the theoretical value [30]. If carbon were indeed present in the RuO_2 NRs, the observed $3d_{5/2}/3d_{3/2}$ integration ratio would show a clear deviation from the ideal value of 3:2. Thus, slow scans over these regions of interest, followed by a least-squares curve fit and deconvolution process to estimate the $3d_{5/2}/3d_{3/2}$ ratio, should give information on the relative carbon content. In this work, no carbon contamination was being detected. The XPS spectra of Ru 3d and O 1s core electrons obtained from RuO_2 NRs on SA(100) are shown in figures 7(a) and (b), respectively. For comparison, the corresponding XPS spectra of a RuO_2 single crystal are also displayed in figures 7(c) and (d), respectively. Both Ru and O 1s core-level spectra for the RuO_2 NRs and single crystal exhibit asymmetric lineshapes; this has been proven to be an intrinsic property in previous study of metallic rutile oxides [31, 32]. The accurate peak positions have been determined by curve fitting using a mixed Gaussian

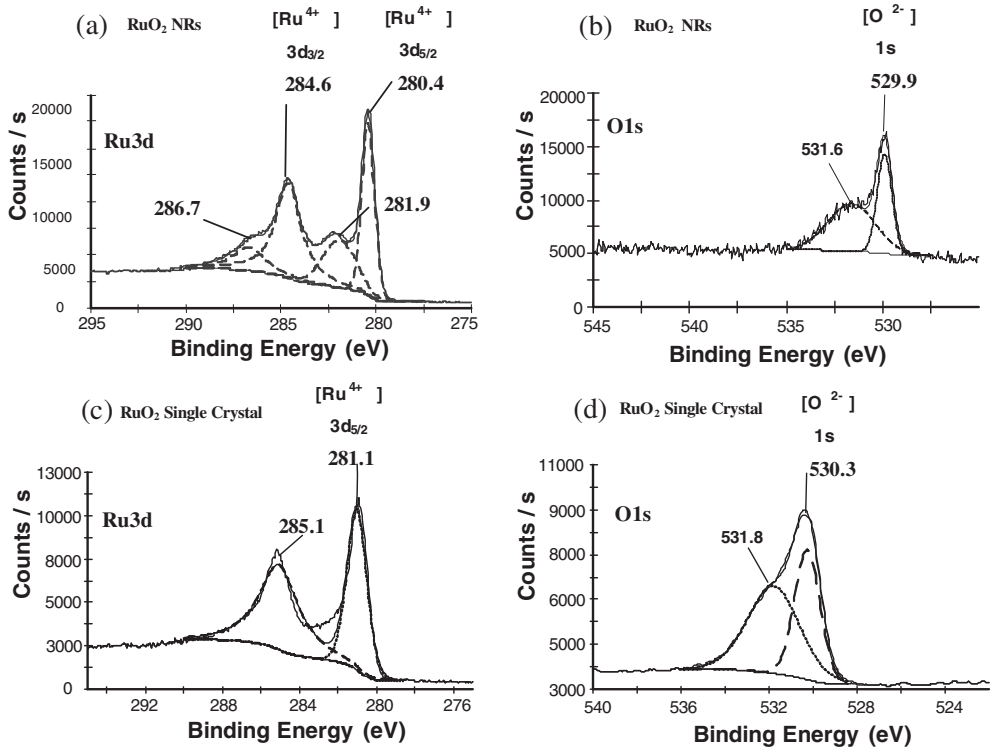

Figure 7. The XP spectra of (a) the Ru 3d line and (b) O 1s line for the RuO_2 nanorods; (c) the Ru 3d line and (d) O 1s line for the RuO_2 single crystal.

and Lorentzian lineshape after treatment of the background with the Shirley function. The Ru 3d signal of the NRs shows the Ru atoms have two different binding states. The peaks identified as $[Ru^{4+}]$ $3d_{5/2}$ and $3d_{3/2}$ at 280.3 and 284.5 eV, respectively, are attributed to the 4+ oxidation state of ruthenium, and are similar to those of the RuO_2 single crystal which are at 280 and 285.1 eV, respectively. Another two broader features at 281.9 and 286.6 eV, which are respectively higher than those of $[Ru^{4+}]$ $3d_{5/2}$ and $3d_{3/2}$ by 1.6 and 2.1 eV, are also observed for the NRs. A similar result is also observed for the O 1s XPS line of the RuO_2 NRs, in which the O 1s signal shows a doublet, similar to the observed for O 1s for the single crystal. The position of the main peak of the doublet at 529.9 eV for NRs is close to that for O 1s for the RuO_2 single crystal (530.3 eV) and an additional broader feature with a higher binding energy of $\sim$531.6 eV is also observed for the NRs. These extra features located at higher binding energy sites of Ru 3d and O 1s might indicate the existence of an impurity with a higher oxidation state in the RuO_2 NRs. Similar spectral features have been observed for RuO_2 films and attributed to the presence of RuO_3 [33]. Quantitative analysis of the peak areas above the background Shirley function, taking into account the sensitivity factors from the Thermo VG Scientific Avantage v1.68 software [26], indicates that the compositions of the NRs are $32 \pm 2\%$ and $68 \pm 2\%$ for Ru and O, respectively. The excess of oxygen during growth is a probable reason for the presence of higher oxidation states of ruthenium. It seems that the occurrence of excess oxygen is a compositional feature of the RuO_2 NRs and the implication of this feature for the growth of RuO_2 NRs is not known at this stage and requires further investigation.

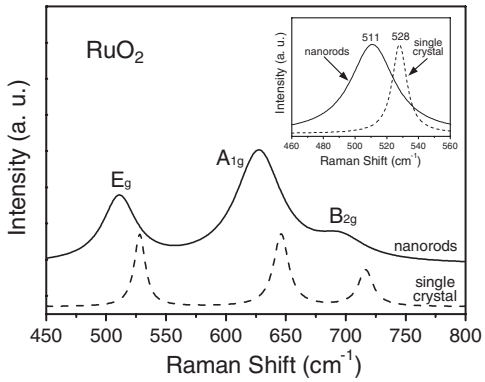

Figure 8. The micro-Raman spectra of the RuO_2 nanorods and RuO_2 single crystal.

Micro-Raman spectroscopy was used to extract microstructural information about the RuO_2 NRs. Figure 8 shows the Raman spectra of the RuO_2 NRs (solid curve) and single crystal (dashed curve) in the range of 450–800 cm^{-1}, in which three Raman modes, identified as E_g, B_{2g}, and A_{1g}, were observed. Analysing the E_g mode (see the inset in figure 8) reveals that the NRs exhibit a 17 cm^{-1} red-shift in peak position (E_g at 511 cm^{-1}) and an asymmetric broadening of 34 cm^{-1} as compared with the single-crystal case, where there was a symmetric line centred at 528 cm^{-1} with linewidth $\sim$12 cm^{-1}. Red-shifts in the Raman peak positions for RuO_2 thin films relative to those of single-crystalline RuO_2 are well known, with a broadening of the peaks as the films become less ordered [34]. The existence of strain in the lattice could also result in a peak shift as well. However, the strain effect is restricted to the interface region and should be minimal for the other parts of the 1D material such as NRs or nanotubes having the least contact area with the substrate. The formation of RuO_2 NRs of single-crystalline quality, as determined from the TEM and XRD studies, also rules out the possibility of any significant disorder in the structure. Accordingly, the results on the peak shift and line broadening should most likely be related to the nanoscale nature of the 1D oxide materials [35], and the phonon confinement effect [36, 37] is probably the mechanism responsible.

4. Summary

RuO_2 NRs have been grown on SA(100) and SA(012) substrates via the MOCVD technique at a deposition temperature of 450 °C and under an oxygen pressure of 10–50 Torr. The results of the structural study reveal that single-crystalline vertically aligned NRs were grown on SA(100), while the NRs on the SA(012) were grown with a tilt angle of $\sim$35° from the normal to the substrates. The RuO_2 NRs showed square cross-sections with the long axis toward the [001] direction. A strong substrate effect on the alignment of the RuO_2 NR growth has been demonstrated and the probable mechanism for the formation of these NRs has been discussed. The presence of ruthenium in a higher oxidation state in the RuO_2 NRs is detected by XPS. The micro-Raman spectrum reveals the presence of a phonon confinement effect in the NRs as manifested by a red-shift and peak broadening of the RuO_2 signatures with respect to the single-crystal case. The results could be useful in providing a new direction for growth control of 1D nanostructures.

Acknowledgment

The authors wish to acknowledge the support of the National Science Council of Taiwan under Contract No NSC 93-2120-M-011-001.

References

[1] Patzke G R, Krumeich F and Nesper R 2002 *Angew. Chem. Int. Edn Engl.* **41** 2446
[2] Xia Y, Yang P, Sun Y, Wu Y, Mayers B, Gates B, Yin Y, Kim F and Yan H 2003 *Adv. Mater.* **15** 353
[3] Huang M H, Mao S, Feick H, Yan H, Wu Y, Kind H, Weber E, Russo R and Yang P 2001 *Science* **292** 1897
[4] Kong Y C, Yu D P, Zhang B, Fang W and Feng S Q 2001 *Appl. Phys. Lett.* **78** 407
[5] Wu J J and Liu S C 2002 *Adv. Mater.* **14** 215
[6] Zhu Y Q, Hu W B, Hsu W K, Terrones M, Grobert N, Hare J P, Kroto H W, Walton D R M and Terrones H 1999 *J. Mater. Chem.* **9** 3173
[7] Kasuga T, Hiramatsu M, Hoson A, Sekino T and Niihara K 1998 *Langmuir* **14** 3160
[8] Jung J H, Kobayashi H, Bommel K J C, Shinkai S and Shimizu T 2002 *Chem. Mater.* **14** 1445
[9] Liu Y, Dong J and Liu M 2004 *Adv. Mater.* **16** 353
Liu Y, Zheng C, Wang W, Yin C and Wang G 2001 *Adv. Mater.* **13** 1883
[10] Bai Z G, Yu D P, Zhang H Z, Ding Y, Wang Y P, Gai X Z, Hang Q L, Xiong G C and Feng S Q 1999 *Chem. Phys. Lett.* **303** 311
[11] Li Y, Bando Y and Golberg D 2003 *Adv. Mater.* **15** 581
Lao J Y, Huang J Y, Wang D Z and Ren Z F 2004 *Adv. Mater.* **16** 65
[12] Choi Y C, Kim W S, Park Y S, Lee S M, Bae D J, Lee Y H, Park G S, Choi W B, Lee N S and Kim J M 2000 *Adv. Mater.* **12** 746
[13] Muhr H J, Krumeich F, Schonholzer U P, Bieri F, Niederberger M, Gauckler L J and Nesper R 2000 *Adv. Mater.* **12** 231
[14] Chen R S, Huang Y S, Liang Y M, Tsai D S, Chi Y and Kai J J 2003 *J. Mater. Chem.* **13** 2525
Chen R S, Huang Y S, Tsai D S, Chattopadhyay S, Wu C T, Lan Z H and Chen K H 2004 *Chem. Mater.* **16** 2457
[15] Wang G, Hsieh C S, Tsai D S, Chen R S and Huang Y S 2004 *J. Mater. Chem.* **14** (Advance article) doi: 10.1039/b409283j
[16] Dziedzic A and Golonka L 1988 *J. Mater. Sci.* **23** 3151
[17] Khanna P K, Bhatnagar S K and Sisodia M L 1988 *J. Phys. D: Appl. Phys.* **21** 1796
[18] Ferro S and de Battisti A 2002 *J. Phys. Chem.* B **106** 2249
[19] Kuhn A T and Mortimer C J 1973 *J. Electrochem. Soc.* **120** 231
[20] Kim T Y, Kim D and Chung C W 1997 *Japan. J. Appl. Phys.* 1 **36** 6494
[21] Bai G R, Tsu I F, Wang A, Foster C M, Murray C E and Dravid V P 1998 *Appl. Phys. Lett.* **72** 1572
[22] Jia Q X and Anderson W A 1990 *Appl. Phys. Lett.* **57** 304
[23] Chen R S, Huang Y S, Liang Y M, Hsieh C S, Tsai D S and Tiong K K 2004 *Appl. Phys. Lett.* **84** 1552
[24] Hsieh C S, Tsai D S, Chen R S and Huang Y S 2004 *Appl. Phys. Lett.* **85** 3860
[25] Satishkumar B C, Govindaraj A, Nath M and Rao C N R 2000 *J. Mater. Chem.* **10** 2115
[26] Thermo VG Scientific: Avantage Software, West Sussex, UK
[27] JCPDS Card No.88-0322, International Centre for Diffraction Data, Newtown Square, PA, USA
[28] JCPDS Card No.10-0173, International Centre for Diffraction Data, Newtown Square, PA, USA
[29] Vetrone J, Foster C M, Bai G R, Wang A, Patel J and Wu X 1998 *J. Mater. Res.* **13** 2281
[30] Feldman L C and Mayer J W 1986 *Fundamentals of Surface and Thin Film Analysis* (New York: North-Holland)
[31] Sarma D D and Rao C N R 1980 *J. Electron Spectrosc. Relat. Phenom.* **20** 25
[32] Wertheim G K and Guggenheim H J 1980 *Phys. Rev.* B **22** 4680
[33] Chan H Y H, Takoudis C G and Weaver M J 1997 *J. Catal.* **172** 336
[34] Bhaskar S, Dobal P S, Majumder S B and Katiyar R S 2001 *J. Appl. Phys.* **89** 2987
[35] Ryan J V, Berry A D, Anderson M L, Long J W, Stroud R M, Cepak V M, Browning V M, Rolison D R and Merzbacher C I 2000 *Nature* **406** 169
[36] Parayanthal P and Pollak F H 1984 *Phys. Rev. Lett.* **52** 1822
[37] Chen R S, Chen C C, Huang Y S, Chia C T, Chen H P, Tsai D S and Tiong K K 2004 *Solid State Commun.* **131** 349